Journal of Molecular Graphics and Modelling 56 (2015) 74–83

Contents lists available at ScienceDirect

Journal of Molecular Graphics and Modelling

journal homepage: www.elsevier.com/locate/JMGM

DFT studies of the formation of furanoid derivatives of ammonium chlorides

Justyna Wielińska, Beata Liberek, Andrzej Nowacki *

Faculty of Chemistry, University of Gdańsk, Wita Stwosza 63, PL-80-308 Gdańsk, Poland

ARTICLE INFO

Article history:
Accepted 16 December 2014
Available online 25 December 2014

Keywords:
Furanoid ring conformation
DFT calculations
NBO
Ammonium salt, Hydrogen bond

ABSTRACT

B3LYP/6-31+G** level computations were performed on the formation of ammonium salts during the reaction of (*S*)-1,4-anhydro-5-chloro-2,3,5-trideoxypentitol (**1**) (*2S*,*5S*)-2,5-anhydro-6-chloro-1,3,4,6-tetradeoxyhexitol (**2**) and methyl 5-chloro-2,3,5-trideoxy-β-D-pentofuranoside (**3**) with ammonia in order to describe the reaction pathway in detail. All the structures were fully optimized in the gas phase, in chloroform and water. In addition, the gas phase activation barrier heights were estimated at B3LYP/6-311++G**, MPWIK/6-31+G**, MPWIK/6-311++G** and MP2/6-311++G(2d,2p)//MPWIK/6-31+G** levels of theory. All the calculations in solvents were performed the using polarizable continuum model (PCM) and the B3LYP functional with the 6-31+G** basis set. A detailed description of all the stationary points is presented, and the conformational behavior of the five-membered ring is discussed in the gas phase and in the solvents. The conversion of the reactant complexes into ion pairs is accompanied by a strong energy decrease in the gas phase and in all the solvents. The overall process is strongly unfavorable in the gas phase, but takes place readily in high-polarity solvents.

1. Introduction

The quaternary ammonium salt (QAS) is the common name for the large group of compounds that have four organic groups covalently bonded to a nitrogen atom. A great diversity of chemical structures is found among QASs, which results mostly from cation. Thus, saturated and unsaturated chains and rings, aromatic residues, and a variety of heterocyclic structures can be found in QASs. Quaternary ammonium salts which have one sugar-derived group attached to the nitrogen atom are also well-known [1,2].

Quaternary ammonium salts are compounds which play an important role in many areas of human activity such as medicine, cosmetics and industry. They exhibit an antibacterial [3–5], antiviral [6,7] and antifungal [8,9] action and are therefore used as disinfectants or for wood preservation [10,11]. One particular type of QASs are ionic liquids (ILs), which have attracted rising interest in the recent decades due to their unique physicochemical properties. Their usefulness as solvents and organic catalysts in chemical synthesis [12], as well as in electrochemistry [13,14] and biochemistry [15–17], was demonstrated.

The quaternization reaction of tertiary amines by alkyl halides, called the Menshutkin reaction (MR) [18], is one of the most universal and convenient methods for obtaining QASs. In this reaction, an electrophilic carbon atom in a halogen derivative is attacked by a nucleophilic nitrogen atom of tertiary amine according to the bimolecular substitution process. Among the many different types of S_N2 reactions which exist the MR is an exceptional one because a charged product is formed from the neutral reactants in it.

The MR has been the subject of extensive theoretical study in recent decades, due to its atypical character [19–31]. The reaction of ammonia, trimethylamine or pyridine and methyl halide represent attractive models of the MR which offer a possibility to study this reaction comprehensively. As a result, these studies have answered many questions concerning this reaction including the role of the leaving group, the nucleophile strength as well as the solvent significance. In particular it has been established that strongly polar solvents facilitate the MR, whereas non-polar solvents stop it, which is a result of the lack of solvation of the transition state geometry and the ionic product.

Obviously, such a simple model is not suitable for investigating the structure–reactivity relationship for the Menshutkin reaction. Thus, in the last few years we have started to focus our studies on the investigation of the structural factors which govern this reaction [32–37]. In particular, we want to evaluate the influence of branching which occurs three bonds distant from the reaction center carbon atom (the hydrogen atom, methyl and methoxyl groups bound to C1 of the tetrahydrofuran (THF)

* Corresponding author. Tel.: +48 585235073.
E-mail address: andrzej.nowacki@ug.edu.pl (A. Nowacki).

http://dx.doi.org/10.1016/j.jmgm.2014.12.004
1093-3263/

ring). We also want to compare the currently presented results with respect to the leaving group and nucleophile, with those obtained earlier [35]. Moreover, we describe the conformational behavior of the THF ring along the reaction pathway. Previously we have presented our results concerning the transformation of chloride derivatives under the trimethylamine action [36]. This time we present our computational studies of the formation of three ammonium salts, analogs to QASs, starting from chloride derivatives ((*S*)-1,4-anhydro-5-chloro-2,3,5-trideoxypentitol (**1**) (*2S,5S*)-2,5-anhydro-6-chloro-1,3,4,6-tetradeoxyhexitol (**2**) and methyl 5-chloro-2,3,5-trideoxy-β-D-pentofuranoside (**3**)) and ammonia, taking place in the gas phase and in two solvents: chloroform and water.

2. Methods

All the calculated structures were prepared in the MOLDEN program [38]. The geometries were initially optimized in the gas phase using the Hartree–Fock (HF) method (6-31G* level). Next, the HF optimized structures were re-optimized using density functional theory (DFT) based on Becke's three parameter hybrid exchange functional [39] involving the gradient-corrected correlation functional of Lee, Yang and Parr [40], with the split-valence basis set including polarized and diffuse functions (B3LYP/6-31+G** method). The reactant complex and transition state geometries were also re-optimized at the B3LYP/6-311++G** level. The reactant complexes and transition states were additionally optimized using MW1K (Pedrew-Wang 1-parameter model for kinetics) [41–43] with two basis sets: 6-31+G**, 6-311++G**. Activation barrier heights were also estimated at the MP2/6-311++G(2d,2p)//MW1K/6-31+G** level of theory. The optimizations were considered satisfactory if the energy difference between the optimization cycles was lower than 1×10^{-6} Hartree and a gradient of $<1 \times 10^{-4}$ a.u. was achieved. The convergence of all the systems studied was checked using harmonic vibrational analysis. No imaginary frequencies were observed for the ground state and there was only one for the transition state. The vibrational analysis also enabled molecular entropies and thermal energy contributions for each conformer to be determined, according to statistical thermodynamics formulae. To discuss the interactions between the constituents of reactant complexes and ion pairs the natural bond orbital (NBO) analysis [44] was carried out at the B3LYP/6-311++G** level.

We used the Self-Consistent Reaction Field SCRF–PCM solvation model [45] to study the influence of solvent on the reaction pathway. The reactions were studied in two media of different polarity, i.e. chloroform ($\varepsilon = 4.9$) and water ($\varepsilon = 78.39$) at the B3LYP/6-31+G** level. The PCM model permits a self-consistent computation of the free energies of solvation, including polarized solute–solvent interactions and non-electrostatic terms in the Hamiltonian. Implicit solvent calculations imply the generation of a vacuum cavity inside a continuous and homogeneous dielectric field. In the PCM model the cavity is built up by a series of interlocking atomic spheres. We used UA0 with scale factor alpha = 1.2 for water and 1.4 for chloroform [29]. Individual spheres were centered on acidic hydrogen atoms. All the DFT calculations were done with the aid of the Gaussian 03 program [46].

3. Results and discussion

3.1. General characteristic of the reaction pathway, exocyclic groups orientation and the furanoid ring conformations

Scheme 1 shows the three reactions that we have been studying. These are considered to proceed through the following pattern: (1) Two separated reactants (denoted as **R**, electrophile – respective chloride derivative and nucleophile – ammonia) approach one another and the van der Waals reactant complex (**RC**) is formed. (2) The constituents of the reactant complex collide to form the transition state (**TS**). (3) The **TS** undergoes a conversion into an ion pair (**IP**). (4) The distance between the ion pair constituents increases to an infinitely great value giving the separated ionic product (**P**).

There are three possible staggered orientations of the chloride atom when the rotation about the C4–C5 bond is considered: *−sc*, *+sc*, *ap* (Fig. 1a). We used the *−sc* C4–C5 bond rotamer in subsequent calculations which we found to be the lowest in energy [36]. This rotamer is the most favorable since the chloride atom is in an antiperiplanar orientation with respect to the ring oxygen atom.

In reaction **3** → **6** the rotation about the O1–C1 bond additionally has to be taken into account (Fig. 1b). Two factors, i.e. steric strains and the *exo*-anomeric effect, govern the rotamer preference here. This effect requires one of the glycosidic oxygen atom lone pairs of electrons to be in an antiperiplanar position with respect to the endocyclic oxygen atom. This requirement is satisfied in *−sc* and *+sc* conformations; however, there are strong steric strains in the latter and therefore is unfavorable. Thus, the *−sc* arrangement is preferred for the rotation about the O1–C1 bond.

The furanoid ring occurs in biopolymers, like DNA and RNA, oligosaccharides and polysaccharides, which are important components of plenty of microorganisms, fungi and plants [47–49]. Because of this the knowledge of the conformational preferences of the furanoid ring is vital for the evaluation of biological activity and chemical reactivity of the compounds consisting of furanoid building elements.

The unsubstituted THF ring simply adopts every conformation met on the pseudorotational pathway and none of them is evidently preferred. However, the introduction to such a ring of one or more non-hydrogen groups affects the energy differentiation of the conformations and makes the ring more "selective" with respect to the adopted conformations. As a consequence, certain conformations are avoided.

The conformations of five-member rings can be described in two complementary ways. Firstly, one can use an illustrative, but less precise *E*/*T* system, where *E* means the envelope and *T* the twist conformation. In the envelope conformation four atoms of the five-member ring are located in a one plane whereas the fifth one is located above or below this plane. In the twist conformation, three consecutive atoms lay in a plane whereas remaining two are shifted out of this plane, one above and the other below. Suitable indexes (superscript or/and subscript) are important to inform which atom(s) is moved out of the plane formed by the remaining atoms. In the envelope conformation the superscript placed before the letter *E* says which atom is located above the plane, whereas the subscript placed after the letter E inform which atom is located below the plan. Similarly, in the twist conformation the superscript placed before the letter *T*, and subscript after this letter indicate which the two atoms are moved above and below the plane, respectively. Secondly, one can describe such a ring shape by defining two parameters introduced by Altona and Sundaralingam (AS), namely the pseudorotational phase angle (*P*) and the puckering amplitude (ϕ_m) [50,51]. The parameter *P* locates the exact position on the pseudorotational circle relative to the arbitrarily chosen conformation, whereas the ϕ_m parameter measures the displacement of an atom(s) out of the plane. Based on a set of five endocyclic torsion angles of a given conformer (ϕ_0–ϕ_4) and using Eq. (1), we can calculate parameter *P*. In turn, the puckering amplitude ϕ_m is related to *P* and ϕ_0 torsion angle through Eq. (2).

$$\tan P = \frac{(\phi_2 + \phi_4) - (\phi_1 + \phi_3)}{3.077\phi_0} \quad (1)$$

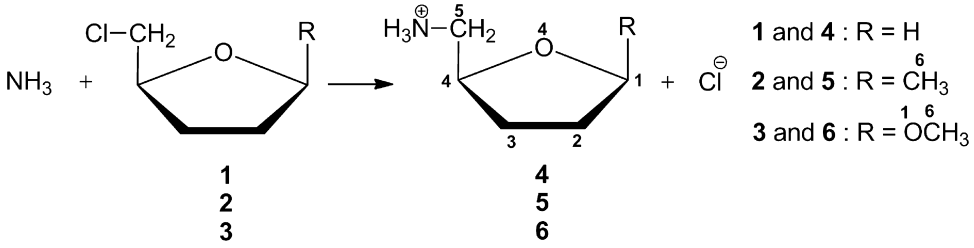

Scheme 1. Reactions of furanoid derivatives of ammonium chloride formation, together with the atom numbering order.

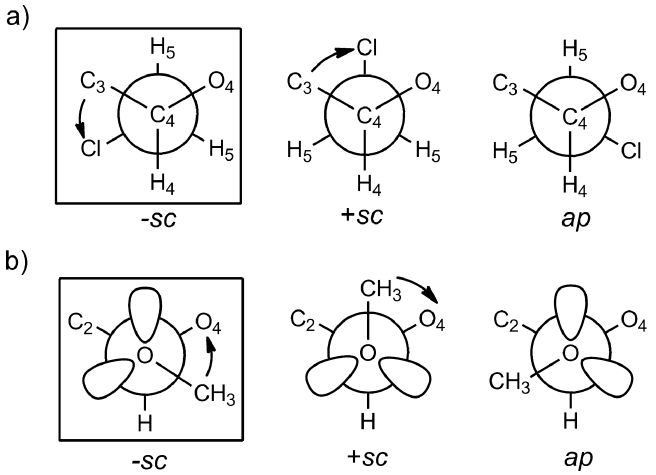

Fig. 1. Staggered rotamers of the C4–C5 bond (a) and the O1–C1 bond (b) exhibiting possible spatial arrangements of exocyclic groups attached to the furanoid ring. The preferred orientations are shown in the boxes.

$$\phi_m = \frac{\phi_0}{\cos P} \quad (2)$$

3.2. Gas phase calculations

3.2.1. Changes in the furanoid ring conformations during the course of the reaction

Both furanoid ring conformation designations (*E* and *T*) and AS parameters (*P* and ϕ_m) values found for the most stable ring shapes, obtained during the optimization, are given in Table 1 together with the set of the endocyclic torsion angles ϕ_0–ϕ_4; the definition of these angles is shown in Fig. 2. The atom numbers are taken from the Scheme 1. Table 1 also lists two torsion angles (χ) describing the spatial disposition of the exocyclic groups attached to the furanoid ring.

In the case of reaction **1** → **4** in the individual reactants the THF ring takes the conformation between E_2 and $^3T_2$ (Table 1) in which the chloromethyl group is in the pseudo-equatorial position with respect to the THF ring ($\chi_1 = -145.2^\circ$). In turn, in the case of reaction **2** → **5** the THF ring adopts preferentially the $^2E/^2T_1$ conformation in which the chloromethyl group is in a pseudo-axial orientation ($\chi_1 = -99.1^\circ$), whereas the methyl group is in a pseudo-equatorial orientation ($\chi_2 = 156.6^\circ$). For the separate chloride derivative in reaction **3** → **6** the calculations showed an E_2 conformation is preferred. In this conformation the chloromethyl group is in the pseudo-equatorial position ($\chi_1 = -138.6^\circ$) and the OCH_3 group is in the pseudo-axial orientation ($\chi_2 = 84.6^\circ$). This preference can be justified based on the *endo*-anomeric effect [52].

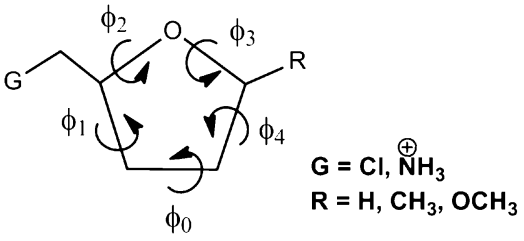

Fig. 2. Definition of the endocyclic torsion angles ϕ_0–ϕ_4.

We did not observe any changes in the THF ring shape for reactant complexes, again $E_2/^3T_2$, $^2E/^2T_1$ and E_2 conformations are found in reactions **1** → **4**, **2** → **5** and **3** → **6**, respectively. Furthermore, the THF ring stays practically unchanged when the reactant complexes convert into the respective transition states in the case of reactions **1** → **4** and **3** → **6**. A certain alteration of the THF ring shape occurs for reaction **2** → **5** ($^2E/^2T_1 \rightarrow {}^2E/^2T_3$).

With one exception, minor, changes in the shape of the THF ring are observed in the course of the conversion of the reactant complex into the respective ion pair. The $E_2/^3T_2 \rightarrow {}^3E$ conformation change is seen for the reaction **1** → **4** whereas in the case of reaction **3** → **6** the THF ring has the same E_2 conformation both in the reactant complex and in the ion pair. The deepest conformational change is observed for the reaction **2** → **5**, where the $^2E/^2T_1$ conformation transforms into the $^0E/^0T_1$ one.

Subsequent conformational changes are observed during the dissociation of the ion pair constituents, minor for reaction **1** → **4** ($^3E \rightarrow {}^3T_2$) and slightly more significant for reaction **2** → **5** ($^0E/^0T_1 \rightarrow {}^2E/^2T_1$). A more elaborate situation is in reaction **3** → **6** where the conformational change occurring during the dissociation process is rather significant ($E_2 \rightarrow {}^4T_0$). We decided to compare the conformation found in reaction **3** → **6** for the individual cation (the $^4T_0$ conformation) with the conformation close to that existing in the ion pair geometry – the $E_2/^1T_2$ conformation (Fig. 3). In the case of the $^4T_0$ conformation the OCH_3 group is in the antiperiplanar orientation in relation to the endocyclic oxygen atom, whereas in the $E_2/^1T_2$ conformation this group is in the *–sc* arrangement, which

Table 1
Selected torsion angles [°] and calculated values of the phase angle pseudorotation *P* and of the puckering amplitude ϕ_m of the THF ring for all stationary points of conversions **1** → **4**, **2** → **5** and **3** → **6** in the gas phase calculated at the B3LYP/6-31+G** level.

		P	ϕ_m	ϕ_0	ϕ_1	ϕ_2	ϕ_3	ϕ_4	χ_1	χ_2
Reaction 1 → 4										
R	$E_2/^3T_2$	352	36	36.0	−27.1	6.7	16.9	−33.1	−145.2	–
RC	$E_2/^3T_2$	351	37	36.2	−26.9	6.1	17.5	−33.4	−145.3	–
TS	$^3T_2$	4	39	39.1	−33.7	15.0	10.2	−31.0	−154.4	–
IP	^3E	16	37	35.4	−35.5	21.7	1.5	−23.7	−153.5	–
P	$^3T_2$	2	37	36.5	−30.9	12.9	10.9	−29.8	−147.9	–
Reaction 2 → 5										
R	$^2E/^2T_1$	153	37	−32.6	17.6	5.6	−26.8	36.5	−99.1	156.5
RC	$^2E/^2T_1$	156	37	−33.7	19.4	3.8	−25.6	36.5	−97.8	156.5
TS	$^2E/^2T_3$	172	37	−36.7	27.4	−7.0	−16.5	33.1	−93.3	153.3
IP	$^0E/^0T_1$	97	41	−5.2	−18.8	37.8	−40.9	27.5	−136.9	147.3
P	$^2E/^2T_1$	149	37	−31.3	14.8	8.5	−28.5	36.5	−101.5	156.1
Reaction 3 → 6										
R	E_2	337	36	33.2	−19.8	−2.6	24.3	−35.7	−138.6	84.6
RC	E_2	340	36	34.1	−21.3	−0.8	23.0	−35.4	−140.4	84.8
TS	$^3T_2$	357	39	38.6	−30.6	10.7	14.1	−32.9	−152.0	38.6
IP	E_2	344	36	34.7	−23.3	1.8	20.9	−34.7	−142.8	85.4
P	$^4T_0$	252	35	−11.1	28.0	−36.4	29.0	−9.8	−91.8	105.8

Definition of the torsion angles: ϕ_0: C1–C2–C3–C4; ϕ_1: C2–C3–C4–O4; ϕ_2: C3–C4–O4–C1; ϕ_3: C4–O4–C1–C2; ϕ_4: O4–C1–C2–C3; χ_1: C5–C4–C3–C2; χ_2: R–C1–C2–C3, R refers the substituent attached to C1.

theoretically should be preferred due to the *exo*-anomeric effect stabilization. Interestingly, the $E_2/^1T_2$ conformation appeared to be less stable (by about 2.3 kcal mol^{-1}) than the $^4T_0$ one. We attributed this to the intramolecular hydrogen bond N—H···O—CH_3, which makes the $^4T_0$ conformation preferred, despite the fact that the metoxy group is in an unfavorable *ap* position.

3.2.2. Energy parameters and geometry changes near the reaction center

The gas phase results of the B3LYP/6-31+G** calculations including activation and reaction energies together with the important geometrical parameters of all the stationary points on a potential energy surface (PES) for reactions **1** → **4**, **2** → **5** and **3** → **6** are presented in Table 2. The calculated total energies were corrected using zero-point vibrational energies (ZPVE), including a scaling factor of 0.9877 [53]. The relative energies refer to the sum of the separate reactant energies. The optimized geometries, together with the relative energies corresponding to all the stationary points along the reaction pathway, are presented in Fig. 4.

The first minimum on the energy curves (Fig. 4) corresponds to the reactant complex (**RC**). In all the cases studied in the gas phase, the approach of the individual reactants is accompanied by a slight energy decrease (see also Table 2). On the other hand, Gibbs free energies predict that the reactant complex formation will be unfavorable in the gas phase (ΔG is about 5.5 kcal mol^{-1}). This suggests that the interaction between the two molecules which form the reactant complex are weak. The constituents of the reactant complex are held together by two hydrogen bonding interactions as revealed by the NBO analysis (Table 3). The suitable second-order perturbation energies $E^{(2)}$ (donor → acceptor) that involve $\sigma^*_{(Y-H)}$ antibonds indicate that the N and O lone pairs participate as donors, whereas the $\sigma^*_{(Y-H)}$ antibonds participate as acceptors in intermolecular charge transfer interactions, $n_X \rightarrow \sigma^*_{(Y-H)}$. All the calculated $E^{(2)}$ values are below 2 kcal mol^{-1} which corroborate that there is a weak attractive interaction between the constituents of the reactant complex.

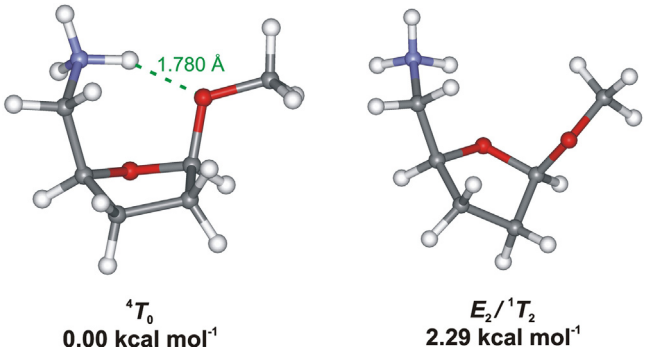

Fig. 3. Comparison of the two individual cation structures calculated for reaction **3** → **6** at the B3LYP/6-31+G** level.

The next stationary point on the potential energy curve corresponds to the transition state (**TS**) geometries. The gas phase relative energy values calculated for TSs are given in Table 2 and in Fig. 4, whereas activation barriers referred to as the reactant complex are listed in Table 4. We have also presented the activation barriers calculated at the B3LYP/6-311++G** level and these obtained using the MPW1K functional and the MP2 method in Table 4. The activation barriers obtained for reactions **1** → **4** and **2** → **5** are comparable whereas it is about 1 kcal mol^{-1} higher for reaction **3** → **6** (33.67, 33.75 and 35.06 kcal mol^{-1} for reaction **1** → **4**, **2** → **5** and **3** → **6**, respectively). One can see that the activation barriers which must be overcome in these reactions, obtained at the MPW1K level, are about 4 kcal mol^{-1} higher than those from the B3LYP level calculations. On the other hand, both functionals slightly underestimate the barrier height, as revealed by a comparison with the MP2 results.

The activation barriers presented in this paper are about 2 kcal mol^{-1} higher than those published previously [35] which is consistent with the weaker basicity of the mesylate anion, hence a better leaving group in the reaction of the nucleophilic substitution. In turn, the comparison of current results with those where trimethylamine served as a nucleophile [36] indicates that the introduction of ammonia in place of trimethylamine does not influence the activation barrier heights considerably.

As Table 2 shows, the geometries of the TSs of reaction **1** → **4**, **2** → **5** and **3** → **6** are very similar. The C···Cl and C···N distances are roughly the same in all TSs (about 2.52 Å and 1.98 Å on average for C···Cl and C···N distances, respectively). The approach of an ammonia molecule to C5 induces a change in the Cl-C5-C4-C3 torsion angle (Table 3). In the reactant complex this angle is close to −70°, whereas in the transition state it takes the values of −20.6°, 0.1° and −30.3° for reactions **1** → **4**, **2** → **5** and **3** → **6**, respectively. Moreover, we noticed that the ClCN valence angles are similar and deviate from the values characteristic of the ideal S_N2 transition state by more than 21°.

Table 2
Geometry parameters, relative energies, relative Gibbs free energies of relevant stationary points on the PES calculated at B3LYP/6-31+G** level for the conversion of **1** → **4**, **2** → **5** and **3** → **6** in the gas phase.

	Reaction **1** → **4**					Reaction **2** → **5**					Reaction **3** → **6**				
	(**R**)	(**RC**)	(**TS**)	(**IP**)	(**P**)	(**R**)	(**RC**)	(**TS**)	(**IP**)	(**P**)	(**R**)	(**RC**)	(**TS**)	(**IP**)	(**P**)
d(C—Cl)	1.819	1.821	2.519	3.536	∞	1.820	1.822	2.533	3.537	∞	1.819	1.821	2.516	3.540	∞
d(C—N)	∞	3.473	1.982	1.489	1.522	∞	3.485	1.982	1.489	1.519	∞	3.483	1.973	1.489	1.521
Δd	−∞	−1.652	0.537	2.047	∞	−∞	−1.664	0.551	2.048	∞	−∞	−1.662	0.543	2.051	∞
∠ ClCN	–	131.4	158.7	51.1	–	–	127.6	157.8	51.1	–	–	128.8	158.6	50.9	–
θ_1	−67.4	−66.6	−20.6	175.6	161.1	−72.6	−71.5	0.1	176.7	158.7	−68.4	−67.1	−30.3	177.3	137.6
θ_2	–	–	164.9	–	–	–	–	166.9	–	–	–	–	162.9	–	–
θ_3	–	–	–	–	–	–	–	–	–	–	−67.0	−65.9	−61.1	−69.2	−157.4
ΔE	0.00	−2.00	31.67	−8.01	105.37	0.00	−1.90	31.85	−8.08	104.49	0.00	−1.73	33.34	−7.94	103.74
ΔG	0.00	5.48	41.00	0.62	107.88	0.00	5.47	41.53	0.65	107.07	0.00	5.65	42.09	1.01	106.51

All energy values in kcal mol^{-1}; d in Å and angles in deg. Reaction coordinate: $\Delta d = d$(C—Cl) − d(C—N).
θ_1 – torsion angle: (Cl–C5–C4–C3) for **R**, **RC** and **TS**; (N–C5–C4–C3) for **IP** and **P**.
θ_2 – deformation angle: C4–C5–H5–H5′ describing the planarity of the transition state geometry [37].
θ_3 – H_3C–O1–C1–O4 torsion angle describing the orientation of the aglycon in relation to the THF ring.

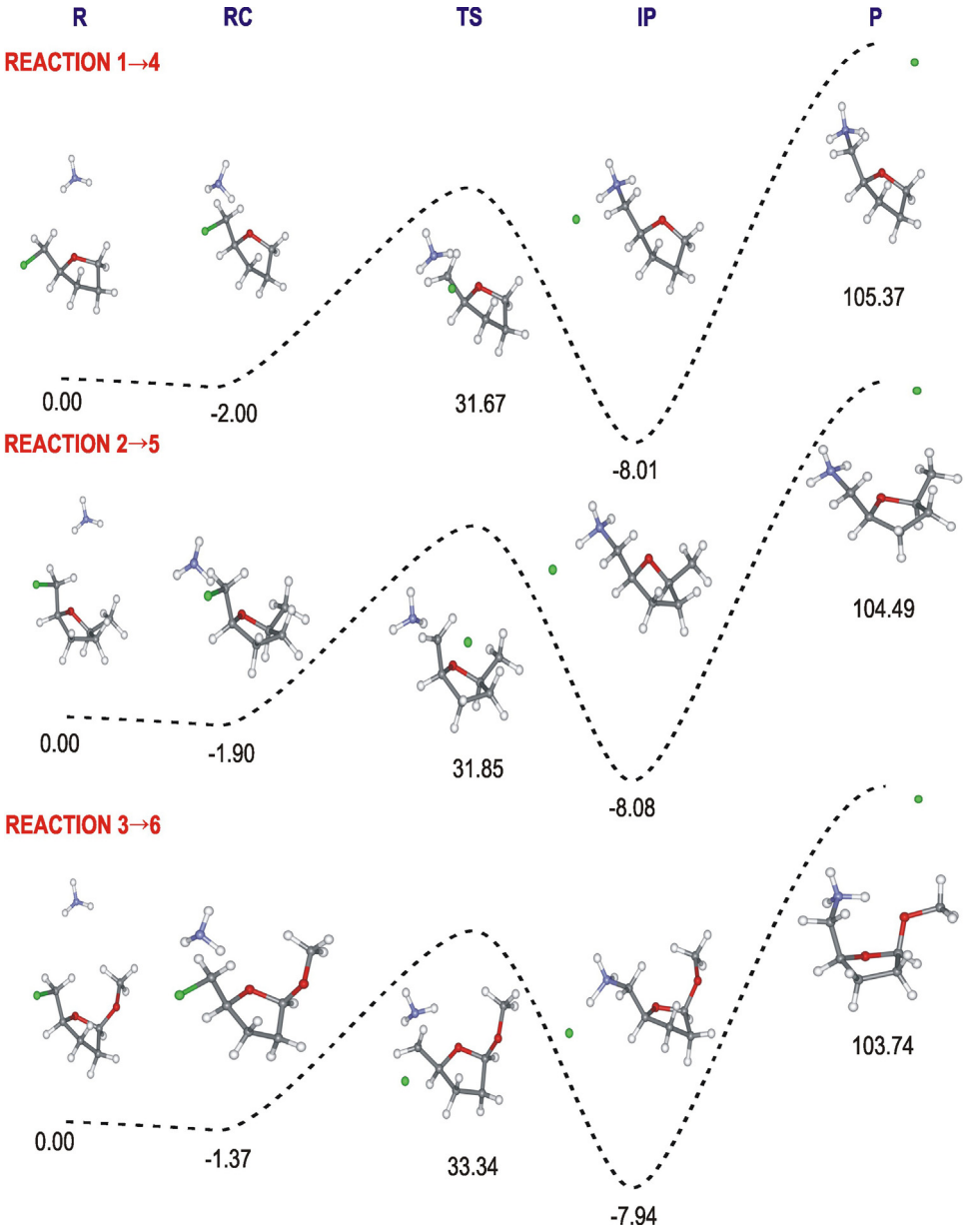

Fig. 4. Geometries of the stationary points and relative energies (kcal mol^{-1}) computed at the B3LYP/6-31+G** level for reactions **1** → **4**, **2** → **5** and **3** → **6** in the gas phase.

Table 3
Geometric parameters, occupation numbers for the $\sigma^*_{(Y-H)}$ antibonds and the n_X lone pairs with their corresponding orbital energies E as well as the second-order perturbation energies $E^{(2)}$ (donor → acceptor) in reactant complexes calculated at the B3LYP/6-31+G** level. X–lone pair donor, Y–H–lone pair acceptor.

	d(H–Y) [Å]	d(X···H–Y) [Å]	d(X···Y) [Å]	∠(X···H–Y) [°]	n_X	E_X [a.u.]	$\sigma^*_{(Y-H)}$	$E_{\sigma^*(Y-H)}$ [a.u.]	$E^{(2)}$ $n_X \rightarrow \sigma^*_{(Y-H)}$ [kcal mol^{-1}]
Reaction 1 → 4									
O(5)···H–N	1.019	2.207	3.134	150.4	1.96664	−0.57367	0.00603	0.46103	1.88
N···H-C(4)	1.091	2.565	3.473	140.4	1.99002	−0.32434	0.02028	0.42280	1.63
Reaction 2 → 5									
O(5)···H–N	1.019	2.217	3.142	150.0	1.96741	−0.57531	0.00583	0.45978	1.77
N···H-C(4)	1.091	2.551	3.485	143.1	1.98971	−0.32415	0.02027	0.42503	1.76
Reaction 3 → 6									
O(5)···H–N	1.018	2.241	3.157	149.1	1.96629	−0.57875	0.00515	0.45593	1.58
N···H-C(4)	1.088	2.594	3.502	140.4	1.99039	−0.32936	0.01986	0.42296	1.53

We have used the C4–C5–H5–H5′ deformation angle (θ_2) to consider the problem of the early/late transition state [37]. As we can see from Table 2, the values of the deformation angle are deviated by about 15° from the ideal S_N2 transition state geometry (180°). These values, in combination with the positive sign, indicate that the transition states have just undergone the Walden inversion (the late transition state).

The second minimum presented in Fig. 4 corresponds to the ion pair (**IP**). In the gas phase, during the conversion of the reactant complex **1**, **2** and **3** into the appropriate ion pair, energy is released (−6.02 kcal mol^{-1}, −6.18 kcal mol^{-1} and −6.21 kcal mol^{-1} in relation to the reactant complex for reactions **1** → **4**, **2** → **5** and **3** → **6**, respectively).

To characterize the interactions which exist between the constituents of the ion pair we have carried out an NBO analysis (Table 5). As previously [37], we expected to see a typical hydrogen bonding interaction accomplished by the transfer of the chloride anion lone pairs electrons onto the $\sigma^*_{(N-H)}$ antibond ($n_{Cl} \rightarrow \sigma^*_{(N-H)}$). However, analysis of the data in Table 5 clearly shows that such an interaction exists only in the case of reaction **1** → **4** but not in reactions **2** → **5** and **3** → **6**. In these two remaining reactions we observe changed connectivity between atoms, i.e. one of the hydrogen atoms of the ammonium cation is transferred to the chloride anion forming the amine hydrochloride (Fig. 5). Therefore, we do not have a real ion pair in reactions **2** → **5** and **3** → **6**. This means that the ion pair formation is followed by the proton transfer in these two cases. We did not observe such a proton transfer in the case of analog reactions with the mesylate leaving group [35]. This is probably, because the mesylate anion is a weaker base than the chloride anion in the gas phase.

The final step of the reaction is the separation of the constituents of the ion pair. As was reported for other reactions, this process is extremely unfavorable in the gas phase. To move the ions an infinite distance from one another there must be more than 100 kcal mol^{-1} supplied in relation to the sum of the energies of the individual reactants (Table 2, Fig. 4).

3.3. Calculations in solution (SCRF-PCM)

3.3.1. Energy parameters and geometry changes

The next step was to examine the influence of environment on the reaction pathway using a polarizable continuum model (PCM) developed by Tomasi and Persico [45]. The reactions were studied in two solvents of different polarity: chloroform and water. The results of the calculations in both solvents are gathered in Table 6, whereas the energy diagrams comparing the energy profiles for the gas phase and solvents are presented in Fig. 6. The energy parameters of the reactions studied in the solvents are expressed by the so-called pseudochemical potential (U_0) [54] and the Gibbs free energy (G).

As can be seen in the presented energy diagrams (Fig. 6) reactions taking place in various environments reveal significant differences. In chloroform, the reactant complexes are less stabilized by about 0.7 kcal mol^{-1} than the respective ones in the gas phase, in comparison with separated reactants. In turn, in water reactant complexes are almost just as stable as individual reactants. However, the Gibbs free energy values clearly indicate that the complexation process is unfavorable in all cases, regardless of the environment it occurs in.

According to the ΔU_0 and ΔG values the conversion of the reactant complex into the ion pair is accompanied by a significant energy decrease in both solvents. For example in water, ion pairs are lower in energy than the respective reactant complexes by at least 17 kcal mol^{-1} (Table 6). In chloroform this effect is not so radical, but is still about 11 kcal mol^{-1}.

As we can see in Table 7, the activation barriers calculated in solvents are lower than those calculated in the gas phase, whereas in Fig. 7 we compared the activation barriers in solvents with those calculated at different levels of theory in the gas phase. For reaction **1** → **4** the barrier ($\Delta G^{\ddagger}$) is lower by 6.1 kcal mol^{-1} when it takes place in chloroform, however in water, the calculated barrier is lower by about 9.2 kcal mol^{-1}. Analogous differences in barrier highs are observed for two other reactions.

The mentioned differences of the barrier height depend on the kind of substituent bonded at the C1 carbon atom, being in *cis* orientation with respect to the reaction center carbon atom (C5). In chloroform and water, the lowest barrier is found for reaction **1** → **4**, in which a hydrogen atom is bonded to the C1. In turn, the highest barrier in both solvents is observed for reaction **3** → **6** (with OCH_3 group at the C1 atom).

We have noticed some changes in the geometry parameters of the transition state during the optimization in solvents. With an increasing polarity of the environment the C···N distance elongates while the C···Cl one shortens, but these changes are not

Table 4
Activation energies calculated for reactions **1** → **4**, **2** → **5** and **3** → **6** in the gas phase. All energy values in kcal mol^{-1}.

	B3LYP				MPW1K				MP2
	6-31+G**		6-311++G**		6-31+G**		6-311++G**		6-311++G(2d,2p)
	$\Delta E^{\ddagger}$	$\Delta G^{\ddagger}$	$\Delta E^{\ddagger}$	$\Delta G^{\ddagger}$	$\Delta E^{\ddagger}$	$\Delta G^{\ddagger}$	$\Delta E^{\ddagger}$	$\Delta G^{\ddagger}$	$\Delta E^{\ddagger}$
1 → 4	33.67	35.52	33.97	35.95	37.67	39.63	38.30	40.39	39.63
2 → 5	33.75	36.06	34.01	36.38	37.71	40.10	38.24	40.76	38.99
3 → 6	35.06	36.45	35.42	37.17	39.37	41.32	40.02	42.21	41.71

Table 5
Geometric parameters, occupation numbers for the n_X lone pairs and the $\sigma^*_{(Y-H)}$ antibonds with their corresponding orbital energies E as well as the second-order perturbation energies $E^{(2)}$ (donor → acceptor) in ion pairs calculated at the B3LYP/6-31+G** level. X–lone pair donor, Y-H–lone pair acceptor.

	d(H–Y) [Å]	d(X···H–Y) [Å]	d(X···Y) [Å]	∠(X···H–Y) [°]	n_X	E_X [a.u.]	$\sigma^*_{(Y-H)}$	$E_{\sigma^*(Y-H)}$ [a.u.]	$E^{(2)}$ $n_X \rightarrow \sigma^*_{(Y-H)}$ [kcal mol^{-1}]
Reaction 1 → 4									
Cl···H–N	1.2034	1.6494	2.8480	173.3	1.99821	−0.77259	0.31421	0.17341	10.60
					1.99534	−0.24876			0.52
					1.99349	−0.24072			0.10
					1.67758	−0.30301			141.86
O···H–N	1.0223	2.3270	2.7814	105.6	1.96916	−0.58784	0.01223	0.34076	0.72
Reaction 2 → 5									
O···H–N	1.0221	2.3488	2.7930	104.9	1.97049	−0.60447	0.01230	0.34007	0.55
N···H–Cl	1.6472	1.2051	2.8479	173.6	1.67021	−0.43803	0.31241	0.13008	193.30
Cl···H–C	1.0998	3.1316	3.8431	123.9	1.99818	−0.77247	0.03525	0.38753	0.06
Reaction 3 → 6									
O···H–N	1.0219	2.3750	2.8208	105.2	1.96870	−0.58994	0.01267	0.33851	0.51
N···H–Cl	1.6369	1.2131	2.8457	173.7	1.67495	−0.43745	0.30801	0.13099	187.84
Cl···H–C	1.0964	3.1308	3.8451	123.4	1.99339	−0.24340	0.02934	0.39435	0.35

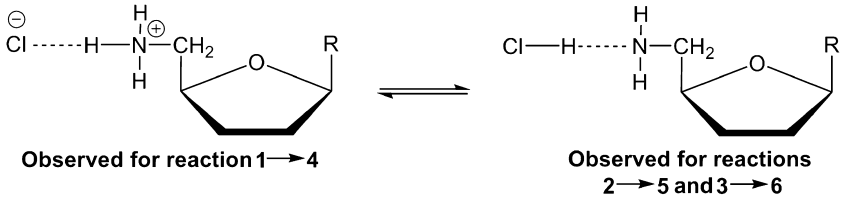

Fig. 5. Proton transfer equilibrium between the ion pair and neutral form.

Table 6
Geometry parameters, relative pseudochemical potentials (ΔU_0), relative Gibbs free energies (ΔG) of relevant stationary points on the FES calculated at the B3LYP/6-31+G** level for the conversions **1** → **4**, **2** → **5** and **3** → **6** in chloroform and water.

	d(C—Cl)	d(C—N)	Δd	∠ ClCN	θ_1	θ_2	θ_3	ΔU_0	ΔG
Chloroform									
Reaction **1** → **4**									
(**R**)	1.823	∞	−∞	–	−67.9		–	0.00	0.00
(**RC**)	1.824	3.517	−1.693	130.9	−68.1		–	−1.24	6.66
(**TS**)	2.443	2.108	0.335	159.2	−8.8	178.8	–	26.12	36.07
(**IP**)	3.637	1.496	2.141	50.8	172.1		–	−12.20	−2.75
(**P**)	∞	1.516	∞	–	164.3		–	26.12	28.40
Reaction **2** → **5**									
(**R**)	1.824	∞	−∞	–	−73.4		–	0.00	0.00
(**RC**)	1.825	3.534	−1.709	127.1	−73.1		–	−1.19	6.64
(**TS**)	2.457	2.102	0.355	158.4	5.7	178.8	–	26.51	36.67
(**IP**)	3.657	1.496	2.161	50.0	172.9		–	−12.12	−2.93
(**P**)	∞	1.514	∞	–	162.4		–	26.05	28.33
Reaction **3** → **6**									
(**R**)	1.823	∞	−∞	–	−68.5		−67.4	0.00	0.00
(**RC**)	1.824	3.520	−1.696	128.0	−67.7		−66.8	−1.05	6.76
(**TS**)	2.448	2.099	0.349	158.8	−11.4	177.5	−66.4	27.35	37.30
(**IP**)	3.640	1.496	2.144	50.4	174.5		−70.7	−11.86	−2.33
(**P**)	∞	1.516	∞	–	141.6		−159.4	27.46	29.99
Water									
Reaction **1** → **4**									
(**R**)	1.827	∞	−∞	–	−68.0		–	0.00	0.00
(**RC**)	1.826	3.842	−2.016	137.2	−68.5		–	−0.39	6.18
(**TS**)	2.379	2.204	0.175	159.4	1.1	−171.2	–	22.66	32.48
(**IP**)	3.782	1.499	2.283	49.3	170.4		–	−17.65	−8.18
(**P**)	∞	1.510	∞	–	167.7		–	−4.84	−1.88
Reaction **2** → **5**									
(**R**)	1.827	∞	−∞	–	−73.9		–	0.00	0.00
(**RC**)	1.827	3.758	−1.931	131.1	−73.8		–	−0.40	6.56
(**TS**)	2.397	2.196	0.201	158.4	14.3	−172.6	–	23.03	32.72
(**IP**)	3.781	1.498	2.283	49.4	166.3		–	−17.73	−8.31
(**P**)	∞	1.509	∞	–	164.0		–	−5.01	−2.01
Reaction **3** → **6**									
(**R**)	1.826	∞	−∞	–	−68.7		−67.3	0.00	0.00
(**RC**)	1.826	3.801	−1.975	131.0	−68.8		−66.9	−0.26	6.44
(**TS**)	2.380	2.201	0.179	159.0	−0.8	−171.6	−66.1	23.34	33.24
(**IP**)	3.765	1.499	2.266	49.7	173.3		−69.9	−17.33	−8.00
(**P**)	∞	1.510	∞	–	170.9		−71.8	−4.09	−1.19

All energy values in kcal mol^{-1}; d in Å and angles in deg. Reaction coordinate: $\Delta d = d$(C—Cl) − d(C—N).
θ_1 – torsion angle: (Cl–C5–C4–C3) for **R**, **RC** and **TS**; (N–C5–C4–C3) for **IP** and **P**.
θ_2 – deformation angle: C4–C5–H5–H5′ describing the planarity of the transition state geometry.[37]
θ_3 – H_3C–O1–C1–O4 torsion angle describing the orientation of the aglycon in relation to the THF ring.

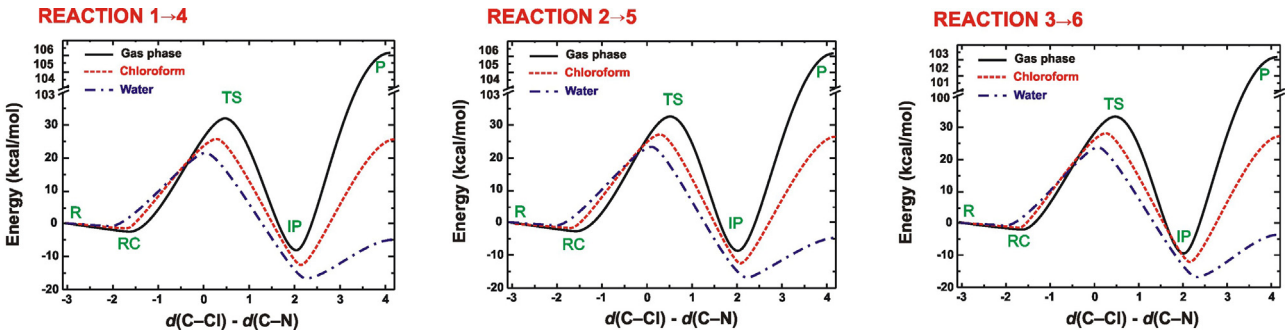

Fig. 6. Comparison of energy (the gas phase) and pseudochemical potential – U_0 (chloroform and water) profiles for reactions **1** → **4**, **2** → **5** and **3** → **6**. Distances are given in [Å].

Table 7
Activation energies calculated at the B3LYP/6-31+G** level for reactions **1** → **4**, **2** → **5** and **3** → **6** in chloroform and water. All energy values in kcal mol^{-1}.

	Chloroform		Water	
	$\Delta E^{\ddagger}$	$\Delta G^{\ddagger}$	$\Delta E^{\ddagger}$	$\Delta G^{\ddagger}$
1 → **4**	27.36	29.41	23.05	26.30
2 → **5**	27.70	30.03	23.43	26.16
3 → **6**	28.40	30.54	23.59	26.79

significant. In the case of reaction **1** → **4** in chloroform the C···N distance increased and the C···Cl distance decreased by about 0.125 Å and 0.076 Å, respectively. In water, these changes were more or less twice as big as in chloroform but are still quite insignificant. These changes undoubtedly indicate that in both solvents, the transition state geometries shift toward the earlier stage of the reaction with respect to the gas phase. Similar conclusions can be drawn when the deformation angle is analyzed (θ_2, Table 6). The values of this angle are still positive but close to 180° in chloroform whereas in water these are negative, therefore the transition state geometries are more reactant-like in both solvents. For the reactions in which the charge separation occurs along the reaction pathway in polar solvents such a behavior of the **TS** geometries is typical.

The separation of the constituents of the ion pair to an infinite distance is the final step of the reaction. This process in the gas phase is strongly endothermic. In turn, in chloroform and water it is much easier, although energy must still be supplied to create the final products. The overall process for the formation of ammonium salts is endoenergetic in chloroform; however, in water environment the energy changes of the charged products are so profound that the reaction is slightly exoergic.

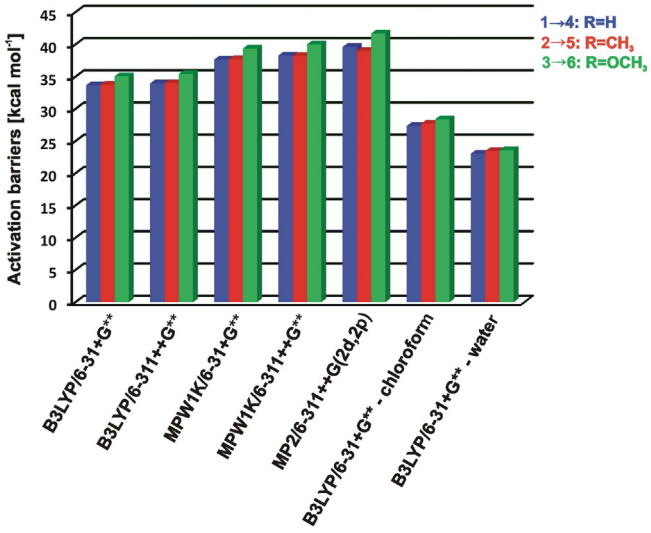

Fig. 7. Comparison of activation energies calculated for reactions **1** → **4**, **2** → **5** and **3** → **6**.

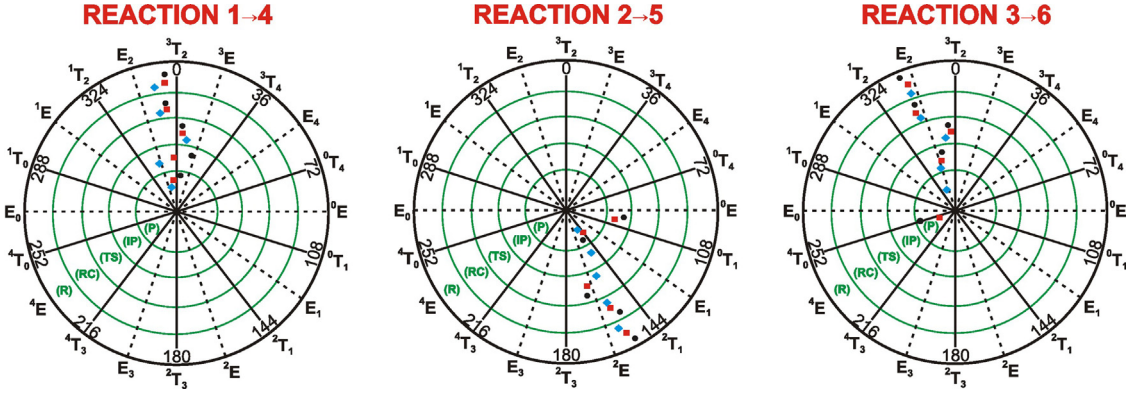

Fig. 8. Distribution of the furanoid ring conformations in a pseudorotational circle for the most stable geometries, calculated at the B3LYP/6-31+G** level, found in the reaction pathways in the gas phase (●) and in solvents: chloroform (■) and water (♦).

3.3.2. Tetrahydrofuran ring conformation in solvents

As we can see in Fig. 8, the optimization in chloroform and water mostly does not change the THF ring conformation. Separate reactants have the same conformation of the THF ring in the gas phase and in solvents. We observed some divergences in the **IP** (reaction **2** → **5**) and individual cation (reaction **3** → **6**) only. Particularly interesting is the situation in the case of the conformational change of the free cation in reaction **3** → **6**. It seems that the intramolecular hydrogen bond N—H···O—CH_3 which stabilized the $^4T_0$ conformation in the gas phase, gets weaker in solvents. In chloroform, this conformation still has lower energy (by about 0.3 kcal mol^{-1}) than the $E_2/^1T_2$; however, the reversed stability of these two conformations is observed in the water environment where the $^4T_0$ conformation has energy 1.50 kcal mol^{-1} higher than the $E_2/^1T_2$ one.

4. Conclusions

In this work we have continued our DFT studies on formation of ammonium salts in a Menshutkin reaction between ammonia and three chloride derivatives. The reactions were analyzed in the gas phase and two solvents: chloroform and water.

We investigated the conformational behavior of the THF ring along the reaction pathway. For reaction **1** → **4** the THF ring conformations oscillate around the north pole of the pseudorotational circle in a range from E_2 to ^3E. In turn, for reaction **2** → **5** the THF ring adopts the conformations in the south-east quarter of the pseudorotational circle (mainly in a region between ^2E and $^2T_1$), whereas in general the E_2 conformation is preferred in the case of reaction **3** → **6**.

The values of energy and Gibbs free energy indicate that the overall process of the formation of ammonium salts is the most unfavorable in the gas phase, in chloroform it is still disadvantageous, however in water the sum of energy of the separated ions is lower than the sum of energy of the separated reagents, so this process is favorable.

Analyzing the potential energy curves we noticed that in the gas phase ion pairs are less stable than the respective reactant complex, however in solvents it is the opposite. Both the energy and the Gibbs free energy values indicate that in chloroform and water, conversion of the reactant complex into the ion pair is accompanied by a significant decrease in energy. The highest decrease in energy took place for reaction **3** → **6** occurring in water, where energy of the ion pair is less by about 15.8 kcal mol^{-1} than the energy of the reactant complex.

In the gas phase the activation barriers for reaction **1** → **4** are lower than for reactions **2** → **5** and **3** → **6**. In turn, the highest activation barrier is for reaction **3** → **6**, where the substituent at the C1 is the OCH_3 group. The same refers to reactions in chloroform and water.

Acknowledgments

This research work was supported by DS/2014 grant. All DFT calculations were carried out using the resources of the Informatics Centre of the Metropolitan Academic Network in Gdańsk (CI TASK).

Appendix A. Supplementary data

Supplementary data associated with this article can be found, in the online version, at http://dx.doi.org/10.1016/j.jmgm.2014.12.004.

References

[1] E. Fischer, K. Raske, Chem. Ber. 43 (1910) 1750–1753.
[2] V. Kumar, C.E. Olsen, S.J.C. Schäffer, V.S. Parmar, S.V. Malhotra, Org. Lett. 9 (2007) 3905–3908.
[3] Y.H. Xiao, J.H. Chen, M. Fang, X.D. Xing, H. Wang, Y.J. Wang, F. Li, J. Oral Sci. 50 (2008) 323–327.
[4] R.T. Carson, E. Larson, S.B. Levy, B.M. Marshall, A.E. Aiello, J. Antimicrob. Chemother. 62 (2008) 1160–1162.
[5] K. Koyama, Y. Shimazu, Drugs and Poisons in Humans, vol. 23, 2005, pp. 407–413.
[6] G. McDonnell, A.D. Russell, Clin. Microbiol. Rev. 12 (1999) 147–179.
[7] V.S. Springthorpe, S.A. Sattar, Crit. Rev. Environ. Sci. Technol. 20 (1990) 169–229.
[8] A.K. Gupta, I. Ahmad, R.C. Summerbell, Med. Mycol. 40 (2002) 201–208.
[9] A. Shirai, T. Sumitomo, M. Kurimoto, H. Maseda, H. Kourai, Biocontrol Sci. 14 (2009) 13–20.
[10] A.P. Ferrell, C.J. Kennedy, A. Wood, B.D. Johnston, W.R. Bennett, Environ. Toxicol. Chem. 17 (1998) 1552–1557.
[11] P.H. McCay, A.A. Ocampo-Sosa, G.T. Fleming, Microbiology 156 (2010) 30–38.
[12] H. Olivier-Bourbigou, L. Magna, D. Morvan, Appl. Catal. A: Gen. 373 (2010) 1–56.
[13] S. Chun, S.V. Dzyuba, R.A. Bartsch, Anal. Chem. 73 (2001) 3737–3741.
[14] A.G. Fadeev, M.M. Meagher, Chem. Commun. 3 (2001) 295–296.
[15] M.H. Abraham, A.M. Zissimos, J.G. Huddleston, H.D. Willauer, R.D. Roger, W.E. Acree, Ind. Eng. Chem. Res. 42 (2003) 413–418.
[16] T. Schafer, C.M. Rodrigues, A.M. Afonso, J.G. Crespo, Chem. Commun. 78 (2001) 1622–1624.
[17] E.D. Bates, R.D. Mayton, I. Ntai, J.H. Davis, J. Am. Chem. Soc. 124 (2002) 926–927.
[18] N. Menschutkin, Z. Phys. Chem. 5 (1890) 589–601.
[19] J.W. Viers, J.C. Schug, M.D. Stovall, J.I. Seeman, J. Comput. Chem. 5 (1984) 598–605.
[20] S.P. Webb, M.S. Gordon, J. Phys. Chem. 103 (1999) 1265–1273.
[21] M. Solà, A. Lledós, M. Duran, J. Bertrán, J.-L.M. Abboud, J. Am. Chem. Soc. 113 (1991) 2873–2879.
[22] J. Gao, X. Xia, J. Am. Chem. Soc. 115 (1993) 9667–9675.
[23] U. Maran, T.A. Pakkanen, M. Karelson, J. Chem. Soc., Perkin Trans. 2 (1994) 2445–2452.
[24] S. Shaik, A. Ioffe, A.C. Reddy, A. Pross, J. Am. Chem. Soc. 116 (1994) 262–273.
[25] X. Fradera, L. Amat, A.M. Torrent, J. Mestres, P. Constans, E. Besalú, J. Martí, S. Simon, M. Lobato, J.M. Oliva, J.M. Luis, M. Andrés, M. Solà, R. Carbó, M. Duran, J. Mol. Struct. Theochem. 371 (1996) 171–183.
[26] T.N. Truong, T.-T.T. Truong, E.V. Stefanovich, J. Chem. Phys. 107 (1997) 1881–1889.
[27] C. Amovilli, B. Mennucci, F.M. Floris, J. Phys. Chem. B 102 (1998) 3023–3028.
[28] H. Castejon, K.B. Wiberg, J. Am. Chem. Soc. 121 (1999) 2139–2146.
[29] J. Poater, M. Solà, M. Duran, X. Fradera, J. Phys. Chem. A 105 (2001) 6249–6257.
[30] A. Fábián, F. Ruff, Ö. Farkas, J. Phys. Org. Chem. 21 (2008) 988–996.
[31] O. Acevedo, W.L. Jorgensen, J. Phys. Chem. B 114 (2010) 8425–8430.
[32] A. Nowacki, B. Dmochowska, E. Jączkowska, K. Sikora, A. Wiśniewski, Comput. Theor. Chem. 973 (2011) 53–61.
[33] A. Nowacki, B. Dmochowska, K. Sikora, J. Madaj, A. Wiśniewski, Comput. Theor. Chem. 986 (2012) 85–92.
[34] A. Nowacki, K. Sikora, B. Dmochowska, A. Wiśniewski, Comput. Theor. Chem. 1000 (2012) 33–41.
[35] A. Nowacki, K. Sikora, B. Dmochowska, A. Wiśniewski, J. Mol. Model. 19 (2013) 3015–3026.
[36] D. Walczak, A. Nowacki, J. Mol. Model. 19 (2013) 4403–4417.
[37] A. Nowacki, J. Wielińska, D. Walczak, K. Sikora, B. Dmochowska, B. Liberek, J. Mol. Graph. Model. 52 (2014) 91–102.
[38] G. Schaftenaar, J.H. Noordik, J. Comput.-Aided Mol. Des. 14 (2000) 123–134.
[39] A.D. Becke, J. Chem. Phys. 98 (1993) 5648–5652.
[40] C. Lee, W. Yang, R.G. Parr, Phys. Rev. B 37 (1988) 785–789.
[41] B.J. Lynch, P.L. Fast, M. Harris, D.G. Truhlar, J. Phys. Chem. A 104 (2000) 4811–4815.
[42] B.J. Lynch, D.G. Truhlar, J. Phys. Chem. A 105 (2001) 2936–2941.
[43] Y. Zhao, J. Pu, B.J. Lynch, D.G. Thuhlar, Phys. Chem. Chem. Phys. 6 (2004) 673–676.
[44] A. Reed, L.A. Curtiss, F. Weinhold, Chem. Rev. 88 (1988) 899–926.
[45] J. Tomasi, M. Persico, Chem. Rev. 94 (1994) 2027–2094.
[46] M.J. Frisch, G.W. Trucks, H.B. Schlegel, G.E. Scuseria, M.A. Robb, J.R. Cheeseman, J.A. Montgomery Jr., T. Vreven, K.N. Kudin, J.C. Burant, J.M. Millam, S.S. Iyengar, J. Tomasi, V. Barone, B. Mennucci, M. Cossi, G. Scalmani, N. Rega, G.A. Petersson, H. Nakatsuji, M. Hada, M. Ehara, K. Toyota, R. Fukuda, J. Hasegawa, M. Ishida, T. Nakajima, Y. Honda, O. Kitao, H. Nakai, M. Klene, X. Li, J.E. Knox, H.P. Hratchian, J.B. Cross, V. Bakken, C. Adamo, J. Jaramillo, R. Gomperts, R.E. Stratmann, O. Yazyev, A.J. Austin, R. Cammi, C. Pomelli, J.W. Ochterski, P.Y. Ayala, K. Morokuma, G.A. Voth, P. Salvador, J.J. Dannenberg, V.G. Zakrzewski, S. Dapprich, A.D. Daniels, M.C. Strain, O. Farkas, D.K. Malick, A.D. Rabuck, K. Raghavachari, J.B. Foresman, J.V. Ortiz, Q. Cui, A.G. Baboul, S. Clifford, J. Cioslowski, B.B. Stefanov, G. Liu, A. Liashenko, P. Piskorz, I. Komaromi, R.L. Martin, D.J. Fox, T. Keith, M.A. Al-Laham, C.Y. Peng, A. Nanayakkara, M. Challacombe, P.M.W. Gill, B. Johnson, W. Chen, M.W. Wong, C. Gonzalez, J.A. Pople, Gaussian 03, Revision D.02, Gaussian, Inc, Wallingford CT, 2004.

[47] J.B. Houseknecht, T.L. Lowary, J. Org. Chem. 67 (2002) 4150–4164.
[48] T.Y. Nikolaienko, L.A. Bulavin, D.M. Hovorun, Phys. Chem. Chem. Phys. 14 (2012) 15554–15561.
[49] H.A. Taha, M.R. Richards, T.L. Lowary, Chem. Rev. 113 (2013) 1851–1876.
[50] C. Altona, M. Sundaralingam, J. Am. Chem. Soc. 94 (1972) 8205–8212.
[51] J.B. Houseknecht, C. Altona, C.M. Hadad, T.L. Lowary, J. Org. Chem. 67 (2002) 4647–4651.
[52] D.J. O'Leary, Y. Kishi, J. Org. Chem. 59 (1994) 6629–6636.
[53] M.P. Andersson, P. Uvdal, J. Phys. Chem. A 109 (2005) 2937–2941.
[54] Y. Kim, J.R. Mohring, D.G. Truhlar, J. Am. Chem. Soc. 132 (2010) 11071–11082.